Adsorption (2008) 14: 165–170
DOI 10.1007/s10450-007-9087-4

Molecular simulation of condensation process of Lennard-Jones fluids confined in nanospace with jungle-gym structure

Satoshi Watanabe · Hayato Sugiyama · Minoru Miyahara

Received: 30 April 2007 / Revised: 28 September 2007 / Accepted: 18 December 2007 / Published online: 4 January 2008

Abstract We report grand canonical Monte Carlo simulations for a Lennard-Jones (LJ) fluid modeled on methane confined in nanospace with jungle-gym-like (JG) cubic structure, which is typically found in porous coordination polymers. Pillars composing the cubic structure were modeled as structureless smooth solid rods made of LJ carbon. We examined the effects of pore size, pore geometry, rod thickness, and rod potential onto the condensation phenomena in the JG pore structure. The simulations clarified that the condensation pressure and adsorption amount in the JG structure were influenced by pore size and rod potential, while the transition type was determined by rod thickness. The characteristics of the JG structure lie in the sensitivity to the slight changes in pore size, rod thickness, and rod potential owing to the combination of the packing effect of molecules and the superposition effect of rod potentials.

Keywords Metal organic frameworks · Condensation phenomena · Jungle-gym cubic nanospace · GCMC simulation

Abbreviations

d pore size of the jungle-gym cubic structure, m
k Boltzmann constant, J·K^{-1}
N number of molecules
p vapor pressure, Pa
p_s saturated vapor pressure, Pa
r interaction distance between molecules or between a molecule and a pillar rod, m
r_c cutoff distance of LJ potential, m
T temperature, K
V volume of the simulation box, m^3
z interaction distance between a molecule and a slit wall, m
Δ separation between lattice planes appeared in (3), m
ε energy parameter in LJ potential, J
ϕ interaction potential, J
μ chemical potential, J
ρ_l line density of atoms in a pillar rod, m^{-1}
ρ_s number density of atoms in solid, m^{-1}
σ size parameter in LJ potential, m

S. Watanabe · H. Sugiyama · M. Miyahara (✉)
Department of Chemical Engineering, Kyoto University, Katsura, Nishikyo, Kyoto 615-8510, Japan
e-mail: miyahara@cheme.kyoto-u.ac.jp

1 Introduction

Phase behavior of fluids confined in nanospace is of great importance to fabricate new porous materials and characterize pore size distributions. A lot of experimental studies have been done to clarify the phase behavior in nanospace. Because microscopic information extracted from experiments is rather limited depending on experimental conditions, computer simulation is an alternative tool to investigate fluid behavior and adsorption mechanisms in nanospace. We have studied condensation (Miyahara et al. 1997, 2000), solidification (Miyahara and Gubbins 1997; Kanda et al. 2000), and sublimation phenomena (Kanda and Miyahara 2007) in slit and cylindrical pores employing the molecular dynamics (MD) and grand canonical Monte Carlo (GCMC) techniques to depict phase diagrams in nanopores in terms of bulk pressure and temperature. Our simulations of freezing/melting transition revealed that freezing point temperature changes dramatically due to the combination of three factors: (i) the compressing effect induced by the pore-wall potential energy, (ii) the geometrical hindrance effect, and

(iii) the tensile effect. For vapor−liquid transition, the combination of the fluid−wall attraction, the shape of meniscus, and curvature-dependence of surface tension plays an important role in determining the critical condensation pressure. As a result, key factors are demonstrated to be the fluid−wall interaction and pore geometry as well as pore size.

Recently, a new class of nanoporous materials called functional porous coordination polymers (Kitagawa et al. 2004) or metal organic frameworks (MOFs) (Yaghi et al. 2003) has been attracting practical interest as well as scientific interest. MOFs, which are composed of metal ions/clusters and bridging organic "pillar" ligands, offer completely new pore geometries of, e.g., one dimensional (1D) square or zigzag channel (Pan et al. 2003; Dybtsev et al. 2004) and 3D interconnected cubic channel (Chui et al. 1999; Eddaoudi et al. 2002) that are never seen in the conventional porous materials such as zeolites and activated carbons. Their important features lie in crystallinity, high surface area, extremely low density, and controllable pore size by changing the length of pillar ligands. Taking advantage of the features, these materials can find applications in materials for gas storage (Noro et al. 2000; Rosi et al. 2003), separation of gas mixture (Kosal et al. 2002; Pan et al. 2006), and heterogeneous catalysis (Seo et al. 2000). Although extensive studies by means of computer simulation (Vishnyakov et al. 2003) as well as experiments have been reported on their structures, adsorption isotherms, storage capacity, and separation selectivity, largely unexplored are phase behaviors of fluids confined in nanospace with pore geometry specific to MOFs. Modeling MOF architectures as well-defined simple shapes would be quite effective to find basic features of fluids confined in the coordination space (Bojan and Steele 1998).

In the present study, we conduct GCMC simulations of a Lennard-Jones (LJ) fluid confined in a simplified "jungle-gym-like" structure of primitive cubic shape with 3D interconnected channels modeled on 3D open frameworks. Pillar ligands composing the 3D frameworks are modeled as uniform solid rods to construct a cubic lattice structure, and the LJ fluid as methane. Condensation phenomena in the jungle-gym cubic structure are studied to explore the effects of the fluid−rod interaction, pore geometry, and pore size.

2 Model and simulation

2.1 Simulation model

The GCMC method (Allen and Tildesley 1987) was used to simulate condensation in a pore system with 3D interconnected channels. Figure 1 shows a jungle-gym-like (JG) simulation box, in which structureless solid rods are placed at even intervals so that they construct a cubic lattice structure. The simulation box was composed of a minimum of $3 \times 3 \times 3$ cubes with the periodic boundary conditions for all directions. The pillar rods were assumed to be made of LJ carbon aligned with a line density ρ_l, which is referred to as the "graphitic rod", and the fluid was LJ methane. The LJ parameters for the graphitic rod and methane were $\sigma_{ss} = 0.340$ nm, $\varepsilon_{ss}/k = 28.0$ K and $\sigma_{ff} = 0.381$ nm, $\varepsilon_{ff}/k = 148.1$ K, respectively. The line density ρ_l was calculated to be $1.955/\sigma_{ss}$ assuming a hexagonal structure of carbon atoms in a graphene sheet.

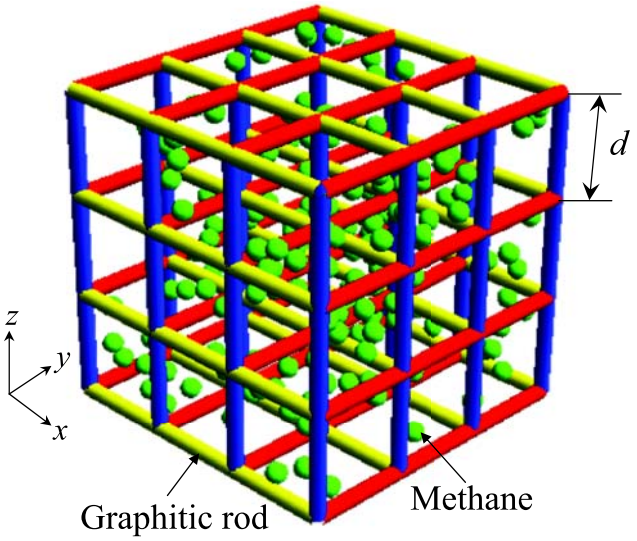

Fig. 1 A schematic drawing of the simulation box

2.2 Potential models

For the fluid−fluid interaction, the LJ 12-6 potential was used:

$$\phi_{ff}(r) = 4\varepsilon_{ff}\left\{\left(\frac{\sigma_{ff}}{r}\right)^{12} - \left(\frac{\sigma_{ff}}{r}\right)^{6}\right\}, \quad (1)$$

where r is the interaction distance. The cutoff distance was set to $r_c = 5\sigma_{ff}$. For the fluid–rod interaction, a "11-5" LJ potential was used, which is derived by a line integral of the 12-6 LJ potential:

$$\phi_{sf}(r) = \frac{3\pi\varepsilon_{sf}\rho_l\sigma_{sf}}{2}\left\{\frac{21}{32}\left(\frac{\sigma_{sf}}{r}\right)^{11} - \left(\frac{\sigma_{sf}}{r}\right)^{5}\right\}, \quad (2)$$

where σ_{sf} and ε_{sf} are the LJ cross parameters for the fluid−rod interaction and given by the Lorentz−Berthelot mixing rules.

As for the potential in structureless slit pore, the so-called 10-4-3 potential was applied:

$$\phi_{\mathrm{slit}}(z) = 2\pi\rho_{\mathrm{s}}\varepsilon_{\mathrm{sf}}\sigma_{\mathrm{sf}}^2\Delta\left[\frac{2}{5}\left(\frac{\sigma_{\mathrm{sf}}}{z}\right)^{10} - \left(\frac{\sigma_{\mathrm{sf}}}{z}\right)^{4} - \left(\frac{\sigma_{\mathrm{sf}}^4}{3\Delta(z+0.61\Delta)^3}\right)\right], \tag{3}$$

where z is the distance between a fluid and the wall surface, ρ_{s} the number density of atoms in the solid, Δ the separation between lattice planes.

2.3 Simulation details

The center-to-center distance between two rods, d, was defined as pore size, and varied from $2\sigma_{\mathrm{ff}}$ to $5\sigma_{\mathrm{ff}}$ in the simulations. The potential profile inside a cube was calculated by superposing the fluid−rod potentials of 1200 rods surrounding the cube, i.e., summing 20 rod contributions for each x, y, z direction. A triple overlap of the fluid−rod potential at an intersection of three rods was corrected by subtracting the overlapped potential obtained by an integral of 12-6 LJ potential along the intersection length which was regarded as the center-to-center distance of LJ atoms. Note that the calculated potential profile inside a cube with the correction showed fairly good accordance with the profile calculated by summation of 12-6 LJ potentials for the same structure but with rods composed of explicit LJ carbon atoms aligned with the same line density ρ_{l}. The potential profile was pretabulated on a 0.05 Å grid, and the potential at each point in 3D space was calculated through interpolation during the simulations.

For the simulations of an adsorption sequence, starting from a sufficiently low relative pressure, the last configuration of a run was used as the initial configuration for the next run with a higher pressure up to a saturated vapor pressure. Alternatively, the configuration of the saturated pressure was used as the starting condition for the next run for a desorption sequence. The relation between the chemical potential μ and the pressure p is given by

$$\mu - \mu_{\mathrm{s}} = kT\ln\left(\frac{p}{p_{\mathrm{s}}}\right), \tag{4}$$

where μ_{s} is the chemical potential corresponding to the saturated vapor pressure p_{s}, k the Boltzmann constant, and T the temperature.

The length of the runs was 40000 steps per molecule, and 1200–2000 molecules were used for liquid state. The overall density ρ^* of fluid in the pore is

$$\rho^* = \rho\sigma_{\mathrm{ff}}^3 \quad \text{with } \rho = \frac{\langle N\rangle}{V}, \tag{5}$$

where $\langle N\rangle$ is the ensemble average of the number of molecules in the pore space and V is the volume of the simulation box including the rod volume.

3 Results and discussion

3.1 Effects of pore size

Figure 2 shows adsorption isotherms at 148.1 K ($T^* = 1.0$) in the JG cubic porous structure for four different pore sizes. For pores of 3, 4, and $5\sigma_{\mathrm{ff}}$, the isotherms show a discontinuous step indicating the pore condensation, while the micropore filling is observed for the case of $d = 2\sigma_{\mathrm{ff}}$. Unfortunately most of the experiments of methane adsorption in MOFs have been conducted under the condition that methane is a supercritical fluid, and consequently the pore condensation has not been so far observed. For the vapor adsorption, however, a discontinuous step in an isotherm has been reported for nitrogen adsorption in a specific type of MOFs (Eddaoudi et al. 2002), and recently the discontinuous step is demonstrated to be due to the pore condensation (Walton and Snurr 2007). Our simulation results are thus consistent with those results, and indicate that the pore condensation occurs in relatively larger pores and that the pore size of $d = 3\sigma_{\mathrm{ff}}$ would be around the boundary that changes adsorption mechanism from the pore condensation to the micropore filling. Note that the hysteresis appeared for $d = 4$ and $5\sigma_{\mathrm{ff}}$ would be an artifact specific to the GCMC method used in the present study, and the true equilibrium must be within the hysteresis loop. The critical condensation pressure shows a monotone decrease with decreasing pore size, which would be due to two contributions: the Kelvin effect on condensation and the effect of the fluid−rod interaction. The adsorption amount also decreases with decreasing

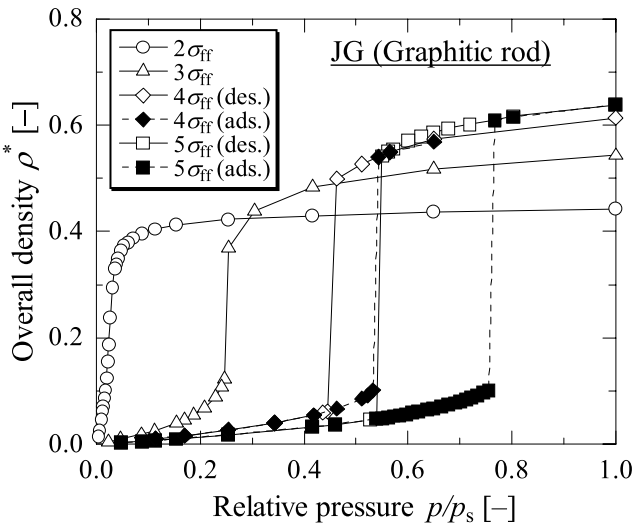

Fig. 2 Simulated adsorption isotherms of LJ methane in the jungle-gym cubic nanopore for four different pore sizes

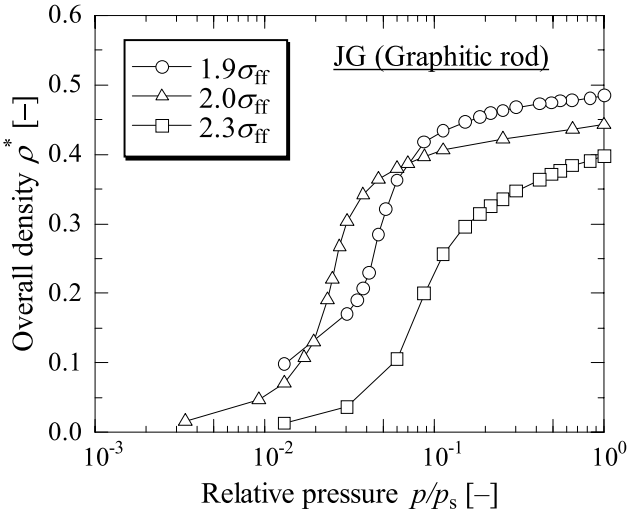

Fig. 3 Same as Fig. 2 but for the pore sizes around $2\sigma_{ff}$

pore size, but the trend is quite different around the pore size as small as $2\sigma_{ff}$, as demonstrated in Fig. 3. The smallest pore size with $d = 1.9\sigma_{ff}$ shows the highest amount among the three. The effect of packing efficiency of molecules would become obvious in this range of pore sizes, in which only about four molecules per cube are accommodated, in addition to the enhancement of the superposition effect of rod potentials.

3.2 Effects of pore geometry

To extract pure effects of pore geometry on the condensation process, we compared the results of JG structures with those of slit pores, both of which are composed of LJ-methane molecules with the same intermolecular potentials and size parameters as used for fluid methane. We set the number density of methane molecules in the slit wall to be $\rho_s = 0.706/\sigma_{ff}^3$ with $\Delta = 1.123\sigma_{ff}$, and the line density in the rod to be $\rho_l = 0.890/\sigma_{ff}$, which are based on the simulation results of bulk phase to calculate the liquid density of LJ-methane at the vapor−liquid equilibrium condition at $T^* = 1.0$. We refer to these as the "methane wall" and "methane rod" respectively. In this condition, the magnitude of the fluid−solid interactions is assumed to be almost the same for the slit pore with methane wall and JG with methane rod. Figures 4(a) and 4(b) show simulated adsorption isotherms in JG with methane rod and slit pore with methane wall. Note that the volume of the slit pore was taken as the space between the planes of the nuclei of the first layer of methane molecules of the walls, which includes some dead space in the vicinity of the walls. No hysteresis was confirmed in the isotherms for the slit pore, while a hysteresis was observed only for $d = 5\sigma_{ff}$ for JG with methane rod. Because the critical condensation pressure would reflect only the Kelvin effect on condensation in the condition of

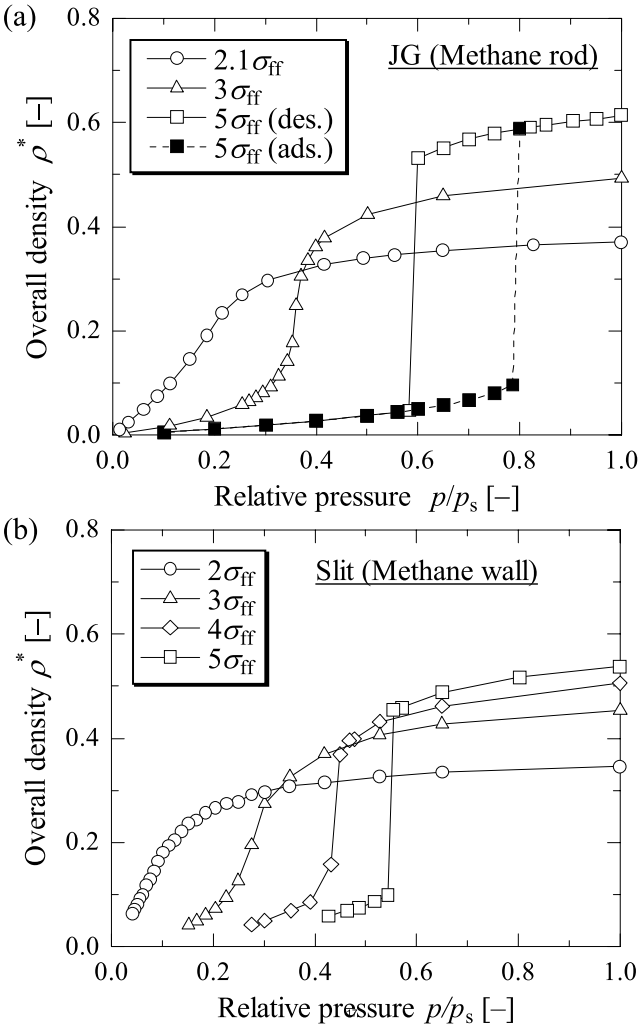

Fig. 4 Simulated adsorption isotherms in (**a**) jungle-gym cubic pore with methane rod and (**b**) slit pore with methane wall for different pore sizes

the fluid−solid potential, the comparison between methane wall slit and methane rod JG would make clear the effect of pore geometry. No sharp vapor−liquid transition occurs for smaller pores of both types as seen from Fig. 4, and the critical condensation pressure is accordingly defined as the inflection point of an adsorption isotherm to make the comparison between the two easy. Figure 5 shows the relation between the critical condensation pressure and the effective pore size defined as surface-to-surface distance between rods or walls, where an error bar indicates the width of a hysteresis loop and the plot placed at the middle of an error bar does not mean true equilibrium. JG with methane rod shows higher condensation pressures than those of slit with methane wall, indicating weaker effects of JG pore geometry onto the condensation process.

JG with graphitic rod, however, exhibits lower condensation pressures than those of slit for smaller pore sizes in spite of similar condensation pressures to those of the

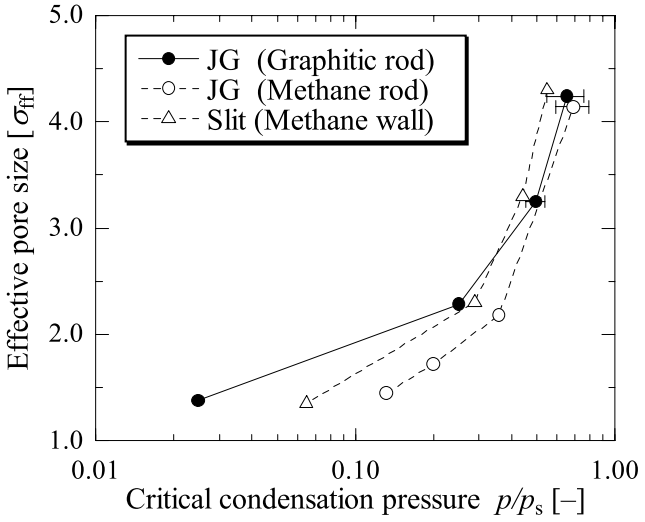

Fig. 5 Relation between the critical condensation pressure and the effective pore size

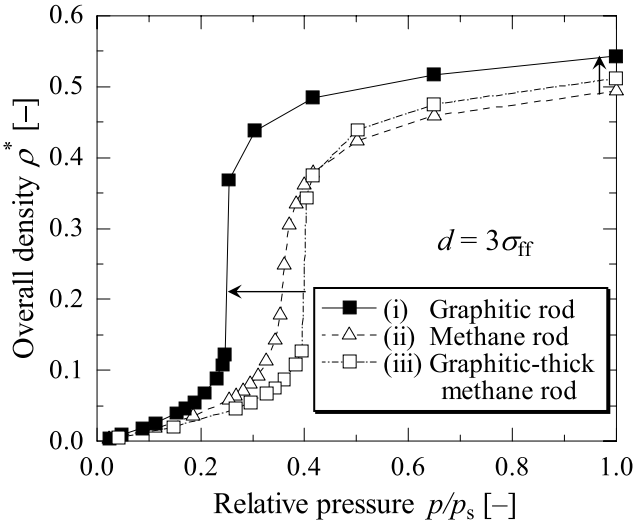

Fig. 6 Comparison of adsorption isotherms for the jungle-gym structures with three different types of rod. The pore size is fixed at $3\sigma_{ff}$

methane rod case for larger pores, as seen in Fig. 5. Stronger fluid−rod interaction relative to fluid−fluid interaction would result in the acceleration of the condensation phenomena in JG with graphitic rod. To evaluate the strength of the fluid−rod interaction, the coefficient $3/2\pi\varepsilon_{sf}\rho_1\sigma_{sf}$ in the 11-5 potential function was calculated for the both cases. Surprisingly, the graphitic rod potential was found to be only 1% greater than that of the methane rod. This sensitivity to the changes in the rod potential is a marked characteristic of the JG structure, which would be caused by strong overlapping of a lot of rod potentials. Note that 1% increase in the wall potential of slit pore gave no significant difference in the condensation pressure compared with that of the methane wall.

Because the graphitic and methane rod have different thickness, to examine separately the effects of the potential and thickness, we compared in Fig. 6 adsorption isotherms in JG with three different types of rods: (i) graphitic rod, (ii) methane rod, and (iii) "graphitic-thick" methane rod that has the same potential as the methane rod and the same thickness as the graphitic rod. The graphitic-thick methane rod gives higher condensation pressure than that of the methane rod, indicating the decrease in the rod thickness leads to the increase in the condensation pressure probably due to the broadening of the pore space. The difference in the adsorption isotherms between the graphitic rod and the graphitic-thick methane rod would thus reflect pure effects of the rod potential, demonstrating that slight increase in the fluid−rod interaction leads to the considerable decrease in the condensation pressure and the increase in the adsorption amount indicated by the arrows in Fig. 6.

Another prominent difference in the adsorption isotherms is the phase transition behavior: the graphitic rod and the graphitic-thick methane rod exhibit the sharp increase at the vapor–liquid equilibrium, while the methane rod gives rather moderate increase. Because the graphitic-thick methane rod gives the pore condensation behavior, the difference in interaction potential between the graphitic rod and the methane rod would not completely explain the difference in the adsorption behavior. Because $d = 3\sigma_{ff}$ is around the boundary of adsorption mechanism as stated in Sect. 3.1, slight increase in the rod thickness would prevent the formation of adsorbed layers around rods by narrowing the space between rods, resulting in the gradual pore filling. Also, the difference in the surface area of rods would be another factor that contributes to the difference in the adsorption behavior. It is surprising that the difference in the rod thickness on the order of 0.1 Å induces the significant change in the transition behavior. As a result, the thickness of the rod is demonstrated to affect the sharpness of the transition for the pore sizes near the boundary between the micropore filling and the pore condensation.

4 Conclusions

We have modeled a MOF structure with interconnected 3D channels as a JG cubic porous structure composed of structureless solid rods, and simulated condensation process in the pore structure using the GCMC method. Through investigating the effects of pore size, pore geometry, and rod potential, we obtained the following conclusions.

(1) The adsorption behavior in the JG structure is quite sensitive to the angstrom-order of difference in the pore size and rod thickness. Pore size affects the critical condensation pressure and adsorption amount. The pore condensation occurs for larger pores, while smaller pores

give the micropore filling. The pore size boundary of adsorption mechanism would be around $3\sigma_{ff}$, and rod thickness plays a role in determining the sharpness of vapor−liquid transition around the boundary pore size.

(2) JG pore geometry has weaker effects on the condensation process than slit shaped pore. However, slight increase in the fluid−rod potential dramatically enhances the condensation especially for small pore size. The sensitivity to the rod potential specific to the JG structure results from the superposition effects of a lot of contributions of rod potentials, which becomes outstanding in the small pore size around $2\sigma_{ff}$.

Acknowledgements This work was supported in part by the Grand-Aid for Scientific Research on Priority Areas, "Chemistry of Coordination Space", by MEXT, Japan.

References

Allen, M.P., Tildesley, D.J.: Computer Simulation of Liquids. Clarendon, Oxford (1987)

Bojan, M.J., Steele, W.A.: Computer simulation in pores with rectangular cross-sections. Carbon **36**, 1417–1423 (1998)

Chui, S.S.-Y., Lo, S.M.-F., Charmant, J.P.H., Orpen, A.G., Williams, I.D.: A chemically functionalizable nanoporous material $[Cu_3(TMA)_2(H_2O)_3]_n$. Science **283**, 1148–1150 (1999)

Dybtsev, D.N., Chun, H., Yoon, S.H., Kim, D., Kim, K.: Microporous manganese formate: a simple metal-organic porous material with high framework stability and highly selective gas sorption properties. J. Am. Chem. Soc. **126**, 32–33 (2004)

Eddaoudi, M., Kim, J., Rosi, N., Vodak, D., Wachter, J., O'keeffe, M., Yaghi, O.M.: Systematic design of pore size and functionality in isoreticular MOFs and their application in methane storage. Science **295**, 469–472 (2002)

Kanda, H., Miyahara, M.: Sublimation phenomena of Lennard-Jones fluids in slit nanopores. J. Chem. Phys. **126**, 054703 (2007)

Kanda, H., Miyahara, M., Higashitani, K.: Solidification of Lennard-Jones fluid in cylindrical nanopores and its geometrical hindrance effect: a Monte Carlo study. Langmuir **16**, 8529–8535 (2000)

Kitagawa, S., Kitaura, R., Noro, S.-I.: Functional porous coordination polymers. Angew. Chem. Int. Ed. **43**, 2334–2375 (2004)

Kosal, M.E., Chou, J.-H., Wilson, S.R., Suslick, K.S.: A functional zeolite analogue assembled from metalloporphyrins. Nat. Mater. **1**, 118–121 (2002)

Miyahara, M., Gubbins, K.E.: Freezing/melting phenomena for Lennard-Jones methane in slit pores: a Monte Carlo study. J. Chem. Phys. **106**, 2865–2880 (1997)

Miyahara, M., Yoshioka, T., Okazaki, M.: Determination of adsorption equilibria in pores by molecular dynamics in a unit cell with imaginary gas phase. J. Chem. Phys. **106**, 8124–8134 (1997)

Miyahara, M., Kanda, H., Yoshioka, T., Okazaki, M.: Modeling capillary condensation in cylindrical nanopores: a molecular dynamics study. Langmuir **16**, 4293–4299 (2000)

Noro, S.-I., Kitagawa, S., Kondo, M., Seki, K.: A new, methane adsorbent, porous coordination polymer $[\{CuSiF_6(4,4'\text{-bipyridine})_2\}_n]$. Angew. Chem. Int. Ed. **39**, 2081–2084 (2000)

Pan, L., Adams, K.M., Hernandez, H.E., Wang, X., Zheng, C., Hattori, Y., Kaneko, K.: Porous lanthanide-organic frameworks: synthesis, characterization, and unprecedented gas adsorption properties. J. Am. Chem. Soc. **125**, 3062–3067 (2003)

Pan, L., Olson, D.H., Ciemnolonski, L.R., Heddy, R., Li, J.: Separation of hydrocarbons with a microporous metal-organic framework. Angew. Chem. Int. Ed. **45**, 616–619 (2006)

Rosi, N.L., Eckert, J., Eddaoudi, M., Vodak, D.T., Kim, J., O'keeffe, M., Yaghi, O.M.: Hydrogen storage in microporous metal-organic frameworks. Science **300**, 1127–1129 (2003)

Seo, J.S., Whang, D., Lee, H., Jun, S.I., Oh, J., Jeon, Y.J., Kim, K.: A homochiral metal-organic porous material for enantioselective separation and catalysis. Nature **404**, 982–986 (2000)

Vishnyakov, A., Ravikovitch, P.I., Neimark, A.V., Bülow, M., Wang, Q.M.: Nanopore structure and sorption properties of Cu-BTC metal-organic framework. Nano Lett. **3**, 713–718 (2003)

Walton, K.S., Snurr, R.Q.: Applicability of the BET method for determining surface areas of microporous metal-organic frameworks. J. Am. Chem. Soc. **129**, 8552–8556 (2007)

Yaghi, O.M., O'keeffe, M., Ockwig, N.W., Chae, H.K., Eddaoudi, M., Kim, J.: Reticular synthesis and the design of new materials. Nature **423**, 705–714 (2003)